metals

MDPI

Article

Effect of Gradient Heat Conduction on Secondary Recrystallization of Grain-Oriented Silicon Steel

Qian Gao [1,2,*], Xianhui Wang [3], Jun Li [1,*], Laifu Cao [3], Jian Gong [3] and Bo Li [1]

[1] Central Iron and Steel Research Institute Group, Beijing 100081, China; lib@cisri.com.cn
[2] Shougang Zhixin Electromagnetic Material R&D (Beijing) Co., Ltd., Beijing 101300, China
[3] Beijing Shougang Co., Ltd., Qian'an 064404, China; wangxianhui@sgqg.com (X.W.); caolf6599@sgqg.com (L.C.); gongjian@sgqg.com (J.G.)
* Correspondence: gaoqian@sgqg.com (Q.G.); junli@atmcn.com (J.L.)

Abstract: The grain-oriented silicon steels were subjected to gradient heat conduction during high-temperature annealing by using thermal insulation cotton. The macrostructures of samples subjected to circumferential gradient heat conduction showed a "petal-like" morphology with peripheral columnar grains and central equiaxed grains, while samples subjected to transverse gradient heat conduction showed a morphology with approximately 50% columnar grains and 50% equiaxed grains. The grain orientations, magnetic domains as well as magnetic properties in different regions were detected. Results showed that the magnetic induction intensity of cylindrical grains was better than that of equiaxed grains while the iron loss was worse, which indicated that a fast heating rate during high-temperature annealing was conducive to the accuracy of Goss grains. The magnetic domains in columnar grains were wider than the equiaxed grains, which resulted in poorer iron loss. A theory of the competitive growth among secondary Goss grains was proposed. Under the condition of gradient heat conduction, once the Goss grains with the fastest heat conduction grew up abnormally, they would compete with other Goss grains which were supposed to survive in traditional processes and swallow up them until adjacent to the secondary equiaxed grains which were later developed.

Keywords: grain-oriented silicon steel; gradient heat conduction; Goss texture; secondary recrystallization; magnetic domain

Citation: Gao, Q.; Wang, X.; Li, J.; Cao, L.; Gong, J.; Li, B. Effect of Gradient Heat Conduction on Secondary Recrystallization of Grain-Oriented Silicon Steel. *Metals* **2024**, *14*, 152. https://doi.org/10.3390/met14020152

Academic Editor: Damien Fabrègue

Received: 5 December 2023
Revised: 17 January 2024
Accepted: 24 January 2024
Published: 26 January 2024

1. Introduction

The grain oriented silicon steel is a kind of soft magnetic functional material, which is mainly used to manufacture the transformer core. It has excellent magnetic performance because of the single and sharp Goss texture {110}<001>, which directly affects the efficiency of power transmission. How to control the secondary recrystallization process to form a perfect Goss texture has been a long-term research focus for grain-oriented silicon steel. The development of secondary recrystallization has a great impact on the magnetic properties of grain-oriented silicon steel. Many studies [1–7] have been conducted on the related factors affecting secondary recrystallization, including key element content, precipitate, primary recrystallization structure, high-temperature annealing process, etc.

In industrial production, secondary recrystallization is developed in the high-temperature annealing furnace, in which coils are annealed vertically. Due to the MgO separator between the steel coil layers, the heat energy is mainly conducted from the end surface of the steel coil to the centre zone along the transverse direction, resulting in inhomogeneous heat conduction. Heat conduction is indeed an important factor in industrial production and has attracted more attention in recent years. Studies [8–11] show that, during the high-temperature annealing process, the grain-oriented silicon steel coil is subjected to uneven heating conditions which are directly related to the different

magnetic properties along the coil. For large ultra-high voltage transformers, it is necessary to obtain raw materials of grain-oriented silicon steel with a uniform microstructure to ensure performance stability. It is therefore essential to investigate the cause of the uneven magnetic properties caused by the heating gradient. This will help to optimise the process.

Furthermore, transformer noise has always been a major environmental concern around the world. The vibration of the transformer core, which causes the noise, is mainly due to the magnetostriction of the grain-oriented silicon steel [12]. In industrial manufacturing, the method of reducing the design magnetic density is generally used to reduce transformer noise, but at the same time, it will significantly increase costs due to increased material consumption. Research [13–16] has shown that in case of the grain-oriented silicon steel with ultra-high magnetic induction intensity, the design magnetic density can be set within the ideal range while achieving lightweight and ultra-low noise transformers. Therefore, there is an urgent need to develop ultra-high magnetic induction intensity grain-oriented silicon steel. Generally, the B_8 (at a magnetic field strength of 800 A/m) of high-grade steel can reach 1.92–1.94 T, while the saturation magnetic induction intensity of Fe-3% Si is about 2.03 T, so there is still potential to increase the value of B_8. In this study, the heat gradient conduction during high-temperature annealing is utilized to achieve ultra-high magnetic induction intensity of grain-oriented silicon steel.

Three main theories have been developed so far on the mechanism of secondary recrystallization of grain-oriented silicon steel [17–19]. (1) Coincident site lattice boundaries theory: The probability of the occurrence of movable coincident site lattice boundaries between the Goss-oriented primary grains and the surrounding grains is the highest. (2) High energy boundaries theory: The probability of the occurrence of movable large-angle grain boundaries between the Goss-oriented primary grains and the surrounding grains is the highest. (3) Solid-state wetting theory: Goss-oriented primary grains infiltrate the adjacent grains by consuming high-energy grain boundaries on the trident nodes. At present, there is still significant controversy over various theories, and further research is needed on the mechanism of secondary recrystallization. The focus of the theoretical debates above has been on the competitive relationship between Goss and other-oriented grains, but there have been no reports on the competitive growth of Goss grains.

The study of gradient heat conduction during high-temperature annealing is therefore of great value both for transformer development and for understanding the mechanism of secondary recrystallization in grain-oriented silicon steel. In this paper, the experiments were specially designed to realize the gradient heat conduction and to study its influence on secondary recrystallization.

2. Materials and Methods

Slab low-temperature reheating grain-oriented silicon steel was smelted by a vacuum induction furnace. The mass fractions of the main chemical components of the test materials are shown in Table 1.

Table 1. The main chemical compositions of the billets (mass fraction, %).

Si	C	Mn	S	Als	N	Fe
3.24	0.062	0.072	0.052	0.025	0.0094	Balance

The billets were heated to 1150 °C × 120 min and then hot-rolled to 2.3 mm. After a two-stage normalizing annealing of 1120 °C × 3 min and 950 °C × 3 min in the N_2 atmosphere, the pickled hot rolling plates were cold rolled to a thickness of 0.27 mm. Subsequently, the decarburizing annealing was performed with the process of 840 °C × 100 s in a wet N_2 and H_2 mixed atmosphere, followed by nitriding annealing with the process of 780 °C × 80 s in an N_2 + H_2 + NH_3 atmosphere. The surface of the nitrided plates was coated with MgO solution and dried immediately, followed by annealing in the high-temperature furnace. During the high-temperature annealing, the samples were first heated

to 950 °C with a heating rate of 20 °C/h and then heated to 1200 °C with a heating rate of 10 °C/h, with the protective atmosphere of 25% N_2 + 75% H_2 before 1100 °C and pure H_2 between 1100–1200 °C. The samples were finally cooled in the furnace with a N_2 atmosphere. The high-temperature annealing process can be seen in Figure 1.

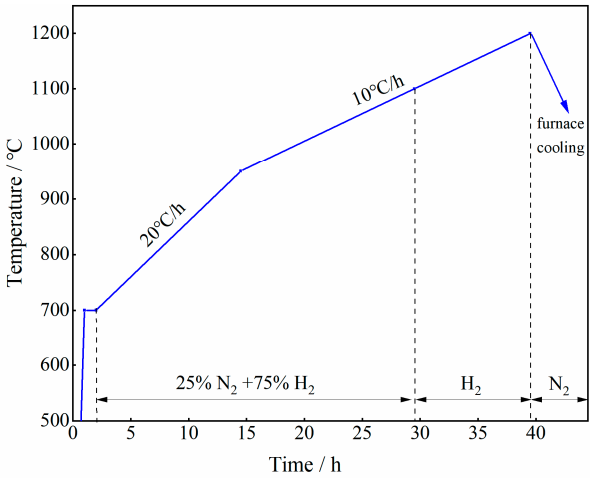

Figure 1. High-temperature annealing process curve.

The samples were subjected to circumferential and transverse gradient heat conductions in high-temperature annealing furnaces by using thermal insulation cotton. The sample size was 420 mm × 300 mm. The thickness of the insulation cotton was 25 mm, and the main components of the insulation cotton were Al_2O_3 and SiO_2. The thermal conductivities at the temperature of 800 °C, 1000 °C and 1200 °C were in the range of 0.23–0.20 W/m·K, 0.32–0.27 W/m·K and 0.43–0.36 W/m·K, respectively. Two sets of experiments were carried out with corresponding samples named S1 and S2. For S1, a layer of insulation cotton measuring 460 mm × 340 mm and 400 mm × 280 mm was placed underneath and on top respectively. There was a 10 mm edge on each of the four sides of the sample that was not covered by the insulation cotton above. The gradient heat conduction in circumferential directions was achieved through this method. For S2, a layer of insulation cotton was also placed underneath and on top, respectively, with dimensions of 500 mm × 350 mm and 500 mm × 330 mm. There was a 10 mm edge along only one side of the sample that was not covered by the insulation cotton above, while the other three edges were fully covered. In this way, the gradient heat conduction along the transverse direction was realized. The schematic diagram of the experimental procedure is shown in Figure 2. During the experiment, three contact thermocouples were used to measure temperatures at each end and centre (points A, B and C in Figure 2d) of the sample.

The grain-oriented silicon steel finally developed a secondary recrystallized structure with large grains. So it was not necessary to use an optical microscope to observe the amplified grain morphology like other small-grain steels. After the samples were taken out of the high-temperature annealing furnace, they were then corroded by hot hydrochloric acid until the glass film was peeled off to reveal the macrostructure. Generally, at a hydrochloric acid concentration of 30% and a hydrochloric acid temperature of 45 °C, the samples were soaked in acid and brushed intermittently for 30 min when a clear macrostructure could be seen with the naked eye. To better display and analyze the overall morphology, a black marker pen was used to trace the visible grain boundaries in the macrostructure.

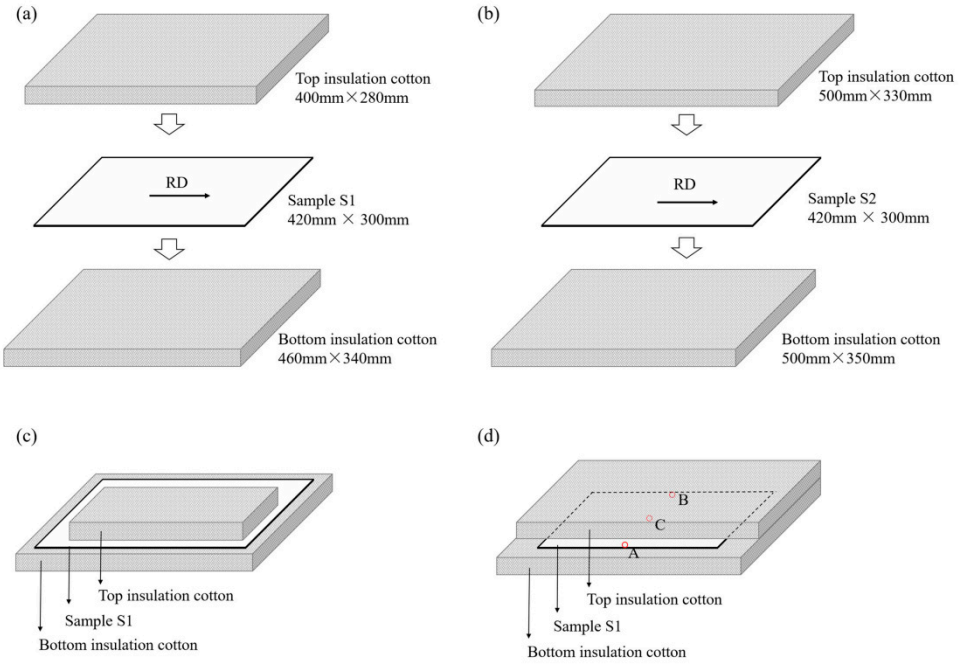

Figure 2. Using thermal insulation cotton to achieve gradient heat conduction during high-temperature annealing (**a**,**c**) Steps of circumferential gradient heat conduction experiment; (**b**,**d**) Steps of transverse gradient heat conduction experiment.

The magnetic properties of samples were tested on the Brockhaus (Wetter, Germany) magnetic property measurement equipment. The magnetic domains were examined using the magnetic powder pattern method. The EBSD detection was performed on a Supra 55 field emission scanning electron microscope from ZEISS company (Jena, Germany). Select a 10 mm × 10 mm sample from the target areas, grind and polish the surface until there are no scratches, then lightly corrode the sample surface with a 3 wt% nitric acid alcohol. After washing and drying the corrosive, the EBSD analysis was carried out.

3. Results

3.1. Macrostructures

Under the conditions of gradient heat conduction, both samples developed secondary recrystallization structures. However, the morphology of the secondary grains was not uniformly equiaxed grains as usual but significantly correlated with the direction of gradient heat conduction. Figure 3 shows the macrostructures of samples, and Figure 4 shows the effect after the grain boundaries were traced with a marker pen.

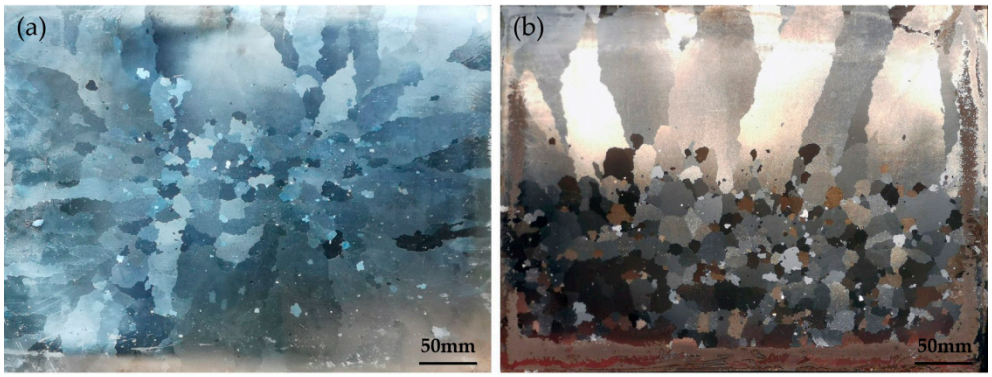

Figure 3. The macrostructures of samples (**a**) S1; (**b**) S2.

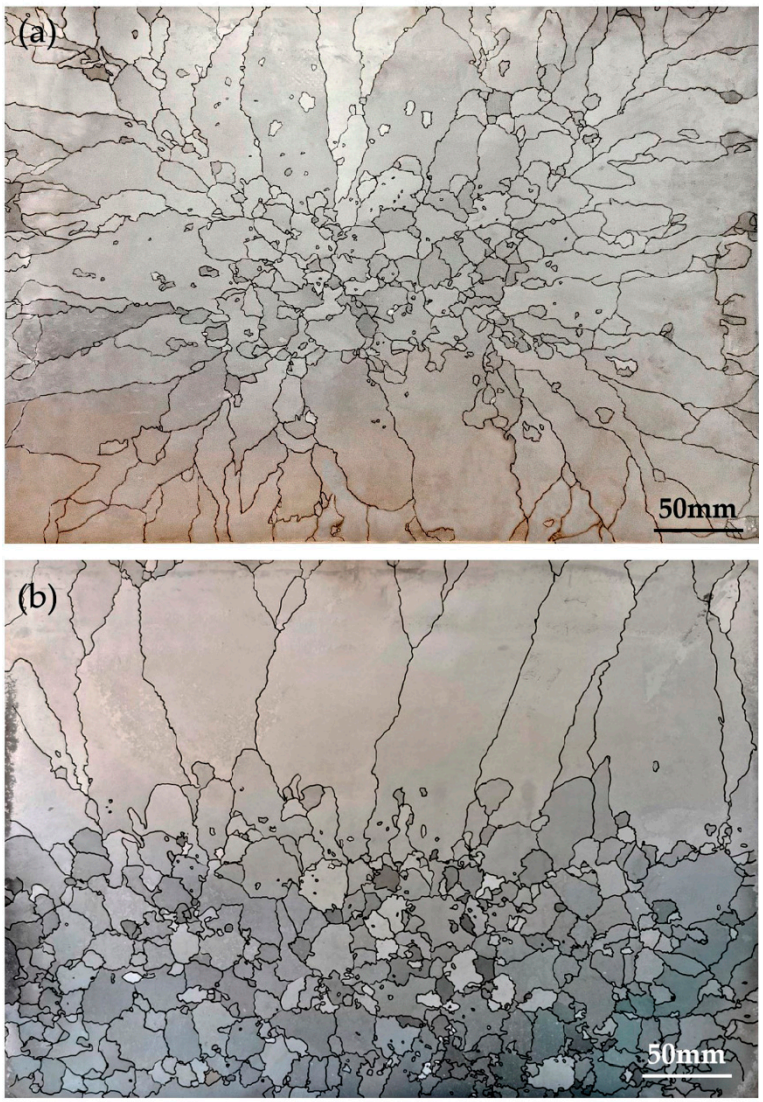

Figure 4. The effect of macrostructures after the grain boundaries were traced by marker pen (**a**) S1; (**b**) S2.

As could be seen from Figures 3 and 4, after high-temperature annealing under the condition of circumferential gradient heat conduction, the surrounding grains of S1 grew into coarse cylindrical grains along the direction of reduced heat conduction velocity, the grain size of which along the long axis direction reached 80–100 mm. In regions where the gradient heat conduction direction coincided with the rolling direction, the grains grew along the rolling direction. In regions where the direction of the gradient heat conduction was the same as the transverse direction, the grains grew along the transverse direction. Particularly, in the corner regions, grains even grew diagonally. It was known that during high-temperature annealing with conventional uniform heat conduction, the grains grew into uniform equiaxed grains. However, after introducing gradient heat conduction, the growing directions of grains in the edge areas were consistent with the gradient heat conduction directions. In the central region, the macrostructures were equiaxed grains with diameters of less than 20 mm. It could be seen that when the coarse columnar grains came into contact with the equiaxed grains in the central region, the migration of columnar grain boundaries along the long axis direction was hindered, so the overall macrostructure of the sample presented a "petal-like" morphology.

For S2, the gradient heat conduction direction was along the transverse direction, resulting in two main regions in the macrostructure. Structures in the region undergoing

fast heat conduction were coarse columnar grains growing along the transverse direction, with a long axis size of about 120–150 mm. Structures in the region experiencing slow heat conduction were equiaxed grains, with diameters less than 20 mm. There was a significant difference and clear boundary between columnar and equiaxed grain regions, with an area ratio of the two regions approximately 1:1.

In addition, the macrostructures of both S1 and S2 had a common characteristic. That was, the secondary recrystallization development for columnar grains got along very well, and the abnormally grown Goss grains could absorb various oriented grains encountered smoothly during their growth process, resulting in few island grains, while the island grains could be found in the equiaxed grain zone.

3.2. Magnetic Properties

Based on the grain morphology characteristic of S1, the magnetic property testing was conducted on typical areas, with a specimen size of 100 mm × 100 mm. The corresponding iron loss $P_{1.7/50}$ (at a frequency of 50 Hz and a maximum magnetic flux density of 1.7 T) and magnetic induction intensity B_{800} are shown in Figure 5. As could be seen the B_{800} of columnar grains was 1.945T–1.967 T, with an average value of 1.955 T, while the B_{800} of the equiaxed grains was 1.919T, indicating that the magnetic induction intensity of columnar grains was significantly better than that of equiaxed grains. Generally, when the macrostructure was consistent, the higher the magnetic induction intensity, the lower the iron loss. However, based on the results of this experiment, the iron loss $P_{1.7/50}$ of columnar grains ranged from 1.085 to 1.249 W/kg, with an average of 1.149 W/kg, while that of the equiaxed grains was 1.022 W/kg, indicating that the iron loss value of columnar grains was to some extent worse than that of equiaxed grains.

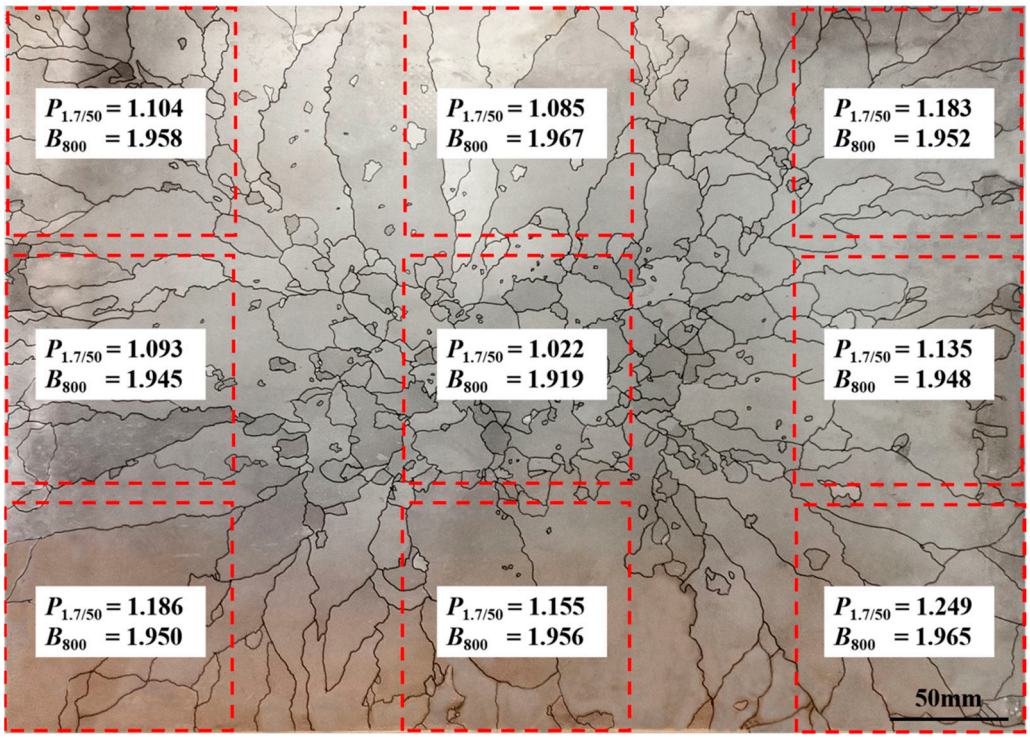

Figure 5. Magnetic properties of typical structures in S1 ($P_{1.7/50}$ in W/kg, B_{800} in T).

Based on the grain morphology characteristics of S2, two samples with the size of 100 mm × 100 mm were cut separately from the typical areas to measure the magnetic performance of $P_{1.7/50}$ and B_{800}, as shown in Figure 6 and Table 2. The data showed that the B_{800} of columnar grains was 1.948 T, while that of equiaxed grains was 1.913 T, indicating that the magnetic induction intensity of columnar grains was significantly better than that

of equiaxed grains. The $P_{1.7/50}$ of columnar grains was 1.117 W/kg, while the value of the equiaxed grains was 1.036 W/kg, which meant that the $P_{1.7/50}$ of columnar grains was 8% higher than that of equiaxed grains. The microstructure characteristics of S2 were consistent with those of S1.

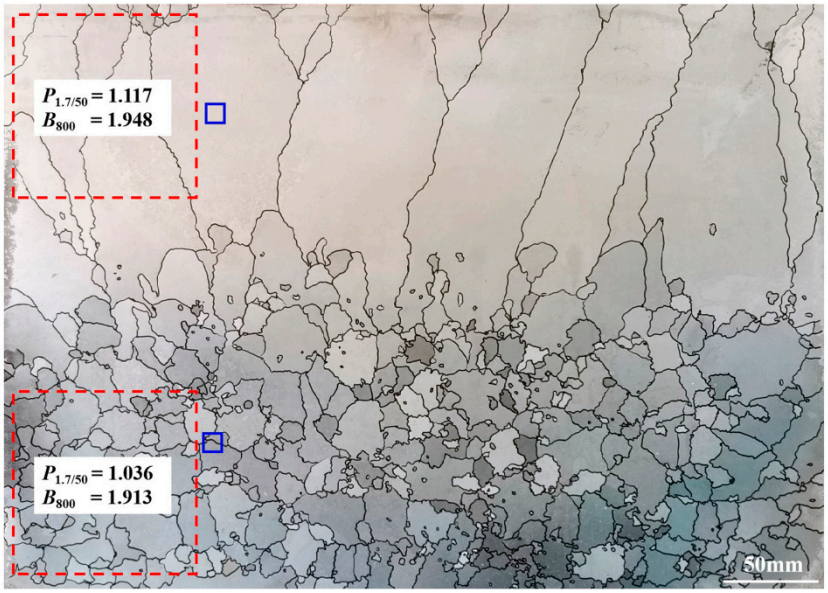

Figure 6. Magnetic properties of typical structures in S2 ($P_{1.7/50}$ in W/kg, B_{800} in T).

Table 2. Magnetic properties of different macrostructure regions in S2.

Macrostructure	$P_{1.7/50}$ (W/kg)	$P_{1.0/2000}$ (W/kg)	B_{800} (T)
Columnar grains	1.117	105.56	1.948
Equiaxed grains	1.036	89.75	1.913

To further obtain the high-frequency iron loss of grains with different morphologies and extend the test specimen coverage, according to the columnar grains and equiaxed grains areas, four pieces of Epstein frame specimens with the size of 30 mm × 300 mm (rolling direction) were processed separately from each area outside the red and blue boxes in Figure 6. The high-frequency iron losses $P_{1.0/2000}$ were measured (at a frequency of 2000 Hz and a maximum magnetic flux density of 1.0 T) and the data were shown in Table 2. It could be seen that the $P_{1.0/2000}$ of columnar and equiaxed grains were 105.56 W/kg and 89.75 W/kg, respectively. The former was higher than the latter, which revealed that the higher the frequency, the more significant the low iron loss advantage of equiaxed grains.

3.3. Grain Orientations

Before high-temperature annealing, the grain morphology and texture of the sample were analyzed by EBSD. Figure 7 shows the typical orientation images and the φ_2 = 45° section of the orientation distribution function (ODF) diagram. As shown in the figure, the nitriding sample was composed of recrystallized equiaxed ferrite grains with an average grain size of 18.3 μm. By determining the grain orientations, it was found that the primary recrystallization textures were mainly composed of {111}<112> (coloured in blue), {114}<481> (coloured in dark green) and {001}<120> (coloured in purple) components and the Goss-oriented grains (coloured in light green) were rarely seen. The grain boundaries between Goss grains and {111}<112>, {114}<481> grains have high mobility [3]. As a result, during the secondary recrystallization in a high-temperature annealing furnace, the {111}<112> and {114}<481> grains would be engulfed by Goss grains.

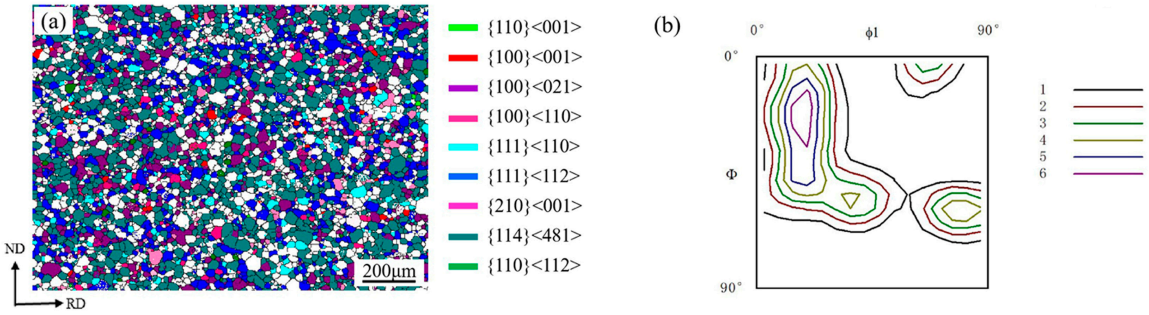

Figure 7. The orientation images (**a**) and φ_2 = 45° section of the orientation distribution function (ODF) diagram (**b**) detected by EBSD before high-temperature annealing.

After high-temperature annealing, typical positions in the equiaxed and columnar crystal regions were selected in S2 for texture testing. The grain orientation calibration and Goss deviation angle are shown in Figure 8, with the blue boxes in Figure 6 representing the locations of the samples tested. Both equiaxed and columnar grains were composed mainly of a single Goss texture (coloured light green). As could be seen in Figures 7 and 8, the scanning areas of each view field observed by EBSD in the primary recrystallized structure and secondary recrystallized structure were the same. Figure 7 showed that there were a large number of primary recrystallized grains in one view field. After the secondary recrystallization, it became only localized single grains in the same area as shown in Figure 8. The secondary grain sizes were thousands or even tens of thousands of times larger than the primary recrystallization sizes.

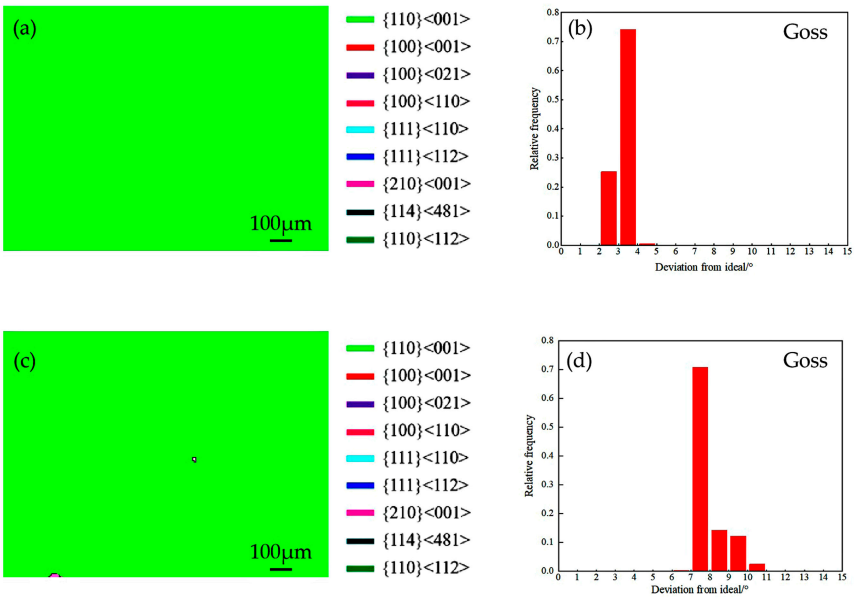

Figure 8. Grain orientation calibration and Goss deviation angles of S2 (**a**,**c**) columnar grains; (**b**,**d**) equiaxed grains.

Figure 8 also showed that the average orientation deviation angle of Goss grains in the columnar grains region was 3.3°, corresponding to a magnetic induction intensity of 1.948 T, while the average orientation deviation angle of Goss grains in the equiaxed grains region was 7.9°, corresponding to a magnetic induction intensity of 1.913 T.

Under the condition of the same Si element content, the magnetic induction intensity was closely related to the deviation angle of the Goss orientation. The more accurate the Goss orientation, the higher the magnetic induction intensity. The data also showed that the correlation between the Goss orientation deviation angle and magnetic induction intensity was more significant than iron loss.

3.4. Magnetic Domains

The spontaneous magnetization directions of iron atoms from different regions in the grains of silicon steel were inconsistent, forming their spontaneous magnetization ranges and becoming magnetic domains. Adjacent magnetic domains were separated by magnetic domain walls. The magnetic powder pattern method was used to test the magnetic domains, as shown in Figure 9.

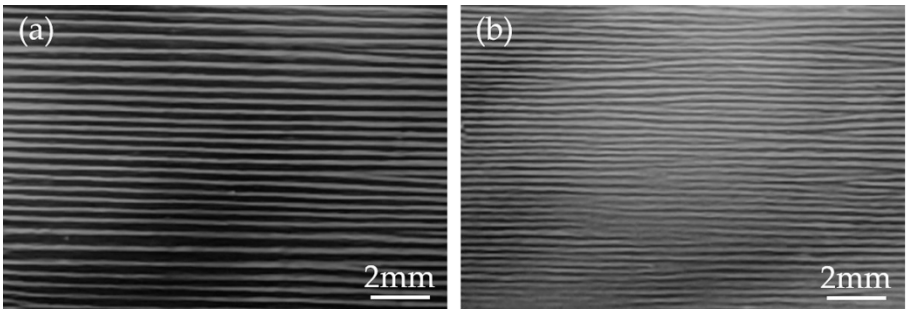

Figure 9. Magnetic domains in different regions of S2 using magnetic powder pattern method (**a**) columnar grains region; (**b**) equiaxed grains region.

For the grain-oriented silicon steel mainly composed of Goss texture, due to the approximate parallel arrangement of the magnetization direction [001] of each grain, the main magnetic domains were mainly 180° sheet-like parallel arranged. It could be seen that the magnetic domains in the columnar grains were coarse, while the secondary grains in the equiaxed grains region were small, resulting in a decrease in the width of the 180° main magnetic domains. The magnetic domain spacing in the columnar grains region was 0.40 mm, while in the equiaxed grains region, it was 0.25 mm. The former was 60% larger than the latter.

4. Discussion

4.1. Effect of Gradient Heating Rate on Secondary Recrystallization

Figure 10 shows the trends of temperature changes over time at different measuring points for S2. It could be seen that the application of thermal insulation cotton caused an uneven heating rate during the high-temperature annealing. The area not covered by thermal insulation cotton, such as point A, had high thermal conductivity efficiency, while the area covered by thermal insulation cotton, such as points B and C, experienced low thermal conductivity efficiency. The farther away from the heat source, the slower the heating was conducted, thus forming a gradient thermal conductivity effect.

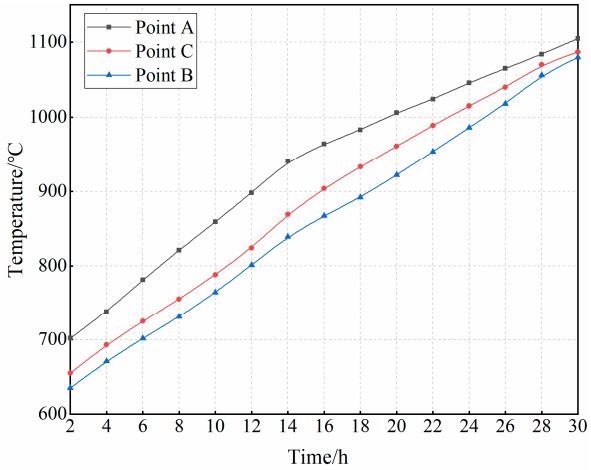

Figure 10. Temperature rise trends over time at different measuring points for S2.

Among the three points measured, the actual temperatures at point A were closest to the set process. During the temperature range of 700–950 °C, the heating rate of the annealing furnace was 20 °C/h. Due to the fast heating rate at point A and the slow heating rate at points B and C, the temperature difference between each point gradually increased. After the process temperature reached 950 °C, the temperature difference between each point gradually decreased due to the decrease in heating rate.

A previous study [4] indicated that the onset secondary recrystallization temperature of grain-oriented silicon steel was about 1020 °C. Point A reached the onset temperature of secondary recrystallization earlier than points B and C. According to the data in Figure 8, during the high-temperature annealing process, the faster the heating rate, the higher the accuracy of the Goss texture, as well as the corresponding magnetic induction intensity. A higher onset secondary recrystallization temperature was conducive to Goss grains with more precise orientation as well as improved magnetic induction intensity [20–22]. Therefore, it could be inferred that the precipitates in the position of point A had a slow decomposition rate due to the fast heating rate of high-temperature annealing, thereby increasing the onset temperature of secondary recrystallization. Even so, according to the grain morphology in Figures 3 and 4, it could be concluded that the position of point A still underwent secondary recrystallization earlier than points B and C.

4.2. Effect of Magnetic Domains on Iron Loss

Iron loss consisted of hysteresis loss P_{h}, eddy current loss P_{e}, and anomalous loss P_{a}. The factors that affected P_{h} were the main obstacles to the movement of magnetic domain walls. When magnetizing repeatedly in an alternating magnetic field, due to the repeated changes in magnetic flux, an induced electromotive force appeared in the change direction of the surrounding magnetic flux, resulting in energy loss caused by the heating of the iron core, which was the eddy current loss. The classical formula for eddy current in thin plate materials derived from Maxwell's equation was expressed in Equation (1) [23].

$$\mathrm{P_e} = \frac{1}{6} \times \frac{\pi^2 t^2 f^2 B_m^2 k^2}{\gamma \rho} \times 10^{-3} \tag{1}$$

where: t was the thickness of the material, f was the frequency, B_{m} represented the maximum magnetic induction intensity, ρ was the electrical resistivity, γ was the density of the material, and k was the waveform coefficient. In this experiment, under the premise of fixed material composition, material thickness and external magnetic induction intensity, the eddy current loss was proportional to f^2.

However, the classical formula mentioned above did not take into account the influence of magnetic domain structure. A previous study [24] showed that all moving domain walls produced the micro-eddy current, and the enhanced eddy-current damping was generated by this synergistic behaviour of complex fine domain structures. Figure 8 indicated that, whether columnar or equiaxed grains, the secondary grains were mainly composed of parallel 180° sheet-like main magnetic domains. The heat loss caused by the eddy current generated by the movement of domain walls was the so-called anomalous loss P_{a}. The time interval for the movement of domain walls was t_{a} to t_{b}, and the movement speed was v. Therefore, the average power loss per unit area P_v was expressed in Equation (2) [25]:

$$\mathrm{P_v} = \frac{1}{\omega} \frac{1}{\mathrm{t}_b - t_a} \int_{t_a}^{t_b} \beta v^2 dt \tag{2}$$

where β was the damping coefficient of the 180° domain wall, and ω was the width of the sample. The domain wall movement velocity is directly proportional to the magnetic domain width, as a result, the anomalous loss P_{a} was enhanced with the increase of magnetic domain width δ.

The finer the division of magnetic domains inside ferromagnetic materials, the lower the static magnetic energy. However, the magnetic domain division led to an increase in the

number of domain walls and an increase in exchange energy. When the increasing domain wall energy exceeded the reducing static magnetic energy, the magnetic domains would no longer be divided, and the total free energy in the system was the lowest. The diameter of columnar grains in S2 was large. Due to the small area occupied by grain boundaries, the hysteresis loss P_h was lower than that of equiaxed grains. However, as shown in Figure 9, the width of magnetic domains corresponding to columnar grains was larger. Therefore, during repeated magnetization, the distance of domain wall movement was longer and the moving speed was faster, causing a higher P_a.

The secondary grains in the equiaxed grains region were small, and the width of the 180° main magnetic domain was narrow. At the same time, there was a large number of island grains in the equiaxed grains region, some of which had the same size as the domain walls, which simultaneously played a role in refining the magnetic domain. Therefore, the P_a in the equiaxed grains was small.

Data in Table 2 showed that at the frequency of 50 Hz, the iron loss of columnar grains was 8% higher than that of equiaxed grains, while at the high frequency of 2000 Hz, it was 18% higher than that of equiaxed grains. That was because the magnetic domain size of coarse grains was large, and under high frequency, eddy currents flew back and forth in the sample. Furthermore, the resistance of the magnetic domain wall to reciprocating motion during service was proportional to the width of the magnetic domain, resulting in the high value of corresponding eddy current loss. Therefore, when applied in the high-frequency field, it would be necessary to control the grain size of the finished product in a smaller range, to reduce the total iron loss.

Many transformers were used in the industrial frequency range, except a few medium and high-frequency special transformers. Lightweight and ultra-low noise transformers had a high demand for magnetic induction intensity. Ultra-high magnetic induction intensity grain-oriented silicon steel could be obtained by increasing the heat conduction gradient. Although the iron loss was to some extent higher, the high magnetic induction intensity could be fully utilized [13–16]. During high-temperature annealing, for coils of 1m width or more, an ultra-high magnetic induction intensity zone of 400–500 mm width would be obtained at the edge of the coil, which was suitable to make ultra-low noise transformers after slitting. For coils less than 500 mm wide, an ultra-high magnetic induction intensity zone could be obtained across the entire width, which would be supplied directly without slitting. By taking advantage of gradient heat conduction, special grain-oriented silicon steel could be developed. On the contrary, measures such as adjusting the position and power of the burners, and optimizing the process curve could be taken to reduce the heat conduction gradient. As a result, the temperature difference between cold and hot temperature spots was reduced and the uniformity of the microstructure was improved. This type of material was found to be suitable for use in large ultra-high voltage transformers.

4.3. Competitive Growth of Secondary Goss Grains

Without the gradient heat conduction, the secondary grains should have grown into uniformly distributed equiaxed grains. However, with the introduction of gradient heat conduction, whether it was circumferential in S1 or transversal in S2, the area not covered by thermal insulation cotton had a faster heating rate, preferentially reaching the onset secondary recrystallization temperature, so induced in the abnormal growth of Goss grains. In addition, the area covered by thermal insulation cotton developed secondary recrystallization later due to a slower heating rate.

Therefore, Goss grains that preferentially experiencing abnormal growth developed into columnar grains by rapidly swallowing the initial recrystallized grains in their adjacent areas along the direction of heat conduction gradient due to their grown-up size advantage, including swallowing Goss grains that should have undergone homogeneous abnormal growth under uniform heat conduction conditions. During the development of columnar Goss grains, the regions with slow thermal conductivity also reached the temperature to develop secondary recrystallization, generating equiaxed grains.

After the coarse columnar grain boundaries migrated to the equiaxed grains region, they could not swallow the already grown equiaxed secondary grains and could not continue to migrate, forming a microstructure where columnar and equiaxed grains coexisted. Based on the above analysis, a model of the competitive growth of secondary Goss grains under gradient heat conduction conditions was established, as shown in Figure 11.

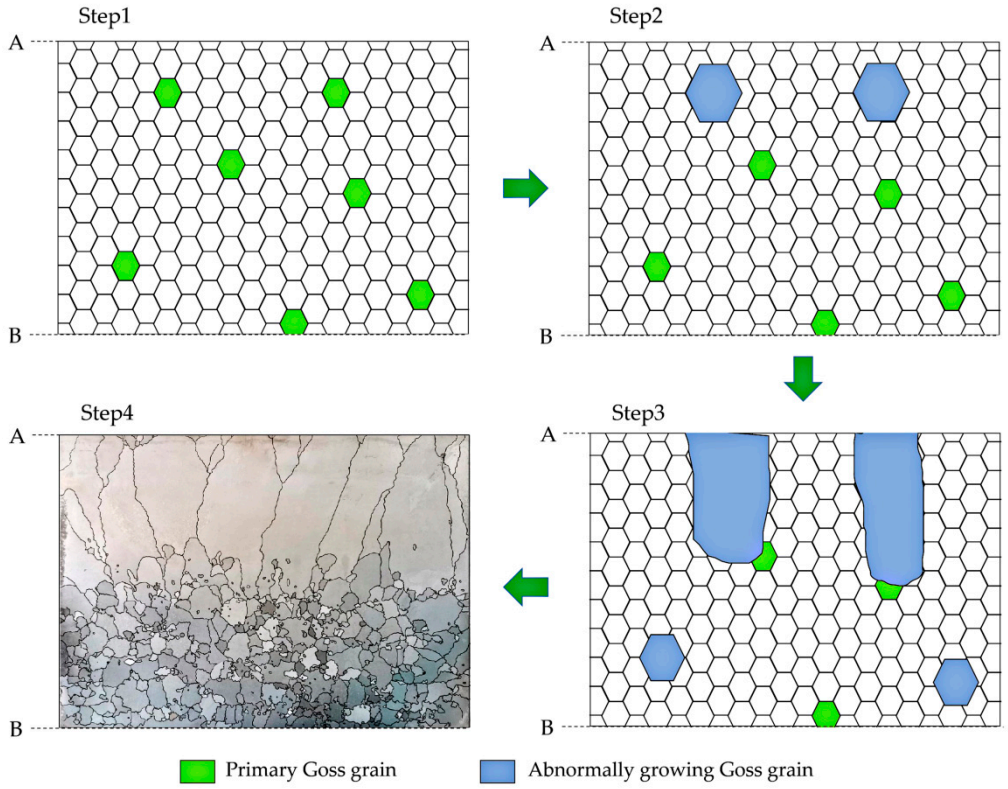

Figure 11. The model of the competitive growth of secondary Goss grains under gradient heat conduction conditions.

According to the model, in the first step, Goss grains were randomly distributed in the primary recrystallization structure, but none of them met the conditions for developing secondary recrystallization. In the second step, Goss grains around point A side started abnormal growth, while the Goss grains around the point B side had not yet experienced abnormal growth. In the third step, the Goss grains around point A side continued to grow along the temperature gradient direction. Along the way, the Goss grains that should have survived were swallowed up. At the same time, the Goss grains around the point B side began to grow abnormally. In the fourth step, the front edge of the Goss columnar grains was adjacent to the equiaxed grains on the point B side, forming the final structure. This indicated that secondary Goss grains with the same crystallographic characteristics also had a competitive relationship under different thermodynamic conditions. With the inducing of external conditions of heat conduction, the competitive advantage of some secondary Goss grains in selectively growing was significantly better than that of conventional Goss grains.

5. Conclusions

1. The circumferential and transverse gradient heat conduction was achieved through the new experimental method of introducing thermal insulation cotton during the high-temperature annealing process of grain-oriented silicon steel. After annealing, columnar and equiaxed grain structures were exhibited simultaneously in the same sample.
2. Under gradient heat conduction conditions, during the high-temperature annealing process, areas with faster heat conduction had a higher heating rate, resulting in

columnar secondary grains, while areas with slower heat conduction had a lower heating rate and equiaxed secondary grains were developed. The orientation deviation angles of Goss grains in the columnar grains were smaller, so the magnetic induction intensity was better than that of equiaxed grains. At the same time, the 180° main domains in the columnar grains were coarser, resulting in higher eddy current loss as well as total iron loss than the equiaxed grains.

3. The competitive growth model of secondary Goss grains during the secondary recrystallization was proposed. After introducing the gradient heat conduction, the Goss grains which were subjected to a higher heating rate developed secondary recrystallization preferentially and further competed with the Goss grains that could have grown abnormally under a uniform heat conduction condition, thus developing into coarse columnar grains.
4. On the one hand, the use of gradient heat conduction could be used to produce ultra-high magnetic induction intensity grain-oriented silicon steel (optimized by 0.03T), which could meet the raw material requirements for ultra-low noise transformers. On the other hand, by reducing the heat conduction gradient of the coil during high-temperature annealing, the occurrence of large grains could be effectively prevented and the uniformity of the microstructure along the coil could be improved, which was beneficial for the application in ultra-high-voltage transformers.

Author Contributions: Conceptualization, J.G.; formal analysis, Q.G. and L.C.; investigation, Q.G. and X.W.; methodology, Li, B.; project administration, X.W.; resources, J.L.; supervision, J.G. and B.L.; writing—original draft, Q.G.; writing—review and editing, L.C. All authors have read and agreed to the published version of the manuscript.

Funding: This research received no external funding.

Data Availability Statement: The raw data supporting the conclusions of this article will be made available by the authors on request.

Acknowledgments: The authors would like to thank Yu Zhao of Central Iron and Steel Research Institute Group for helpful discussions on topics related to this work.

Conflicts of Interest: Author Qian Gao was employed by the company Shougang Zhixin Electromagnetic Material R&D (Beijing) Co., Ltd. Authors Xianhui Wang and Laifu Cao were employed by the company Beijing Shougang Co., Ltd. The remaining authors declare that the re-search was conducted in the absence of any commercial or financial relationships that could be construed as a potential conflict of interest.

References

1. Xu, Z.; Sha, Y.; Zhang, F.; Zhang, H.; Li, G.; Chu, S.; Zuo, L. Orientation Selection Behavior During Secondary Recrystallization in Grain-Oriented Silicon Steel. *Acta Metall. Sin.* **2020**, *56*, 1067–1074. [CrossRef]
2. Xu, Z.; Sha, Y.; He, Z.; Zhang, F.; Liu, W.; Zhang, H.; Zuo, L. Complete Goss secondary recrystallization by control of the grain size and texture of primary recrystallization in grain-oriented silicon steel. *Materials* **2021**, *14*, 5383. [CrossRef] [PubMed]
3. Gao, Q.; Wang, X.; Li, J.; Gong, J.; Li, B. Effect of aluminum on secondary recrystallization texture and magnetic properties of grain-oriented silicon steel. *J. Iron Steel Res. Int.* **2021**, *28*, 47–487. [CrossRef]
4. Gao, Q.; Li, J.; Wang, X.; Gong, J.; Li, B. Characteristic of Precipitate Evolution during High Temperature Annealing in Grain-Oriented Silicon Steel. *Metals* **2022**, *12*, 824. [CrossRef]
5. Wang, Y.; Zhu, C.; Li, G.; Liu, Y.; Liu, Y. Influence of Nb content on precipitation, grain microstructure, texture and magnetic properties of grain-oriented silicon steel. *Materials* **2020**, *13*, 5581. [CrossRef]
6. Liu, G.; Yang, P.; Mao, W. Effect of final annealing atmosphere on secondary recrystallization behavior in thin gauge medium temperature grain oriented silicon steel. *Acta Metall. Sin.* **2016**, *52*, 25–32. [CrossRef]
7. Petryshynets, I.; Kováč, F.; Petrov, B.; Falat, L.; Puchý, V. Improving the Magnetic Properties of Non-Oriented Electrical Steels by Secondary Recrystallization Using Dynamic Heating Conditions. *Materials* **2019**, *12*, 1914. [CrossRef] [PubMed]
8. Xia, T.; He, Z.; Luo, Z. The Heat Transfer Model of Oriented Silicon Steel Coil in Annular Furnace during the Heating Stage of High-Temperature Annealing. *Steel Res. Int.* **2021**, *92*, 2000290. [CrossRef]
9. Xia, T.; He, Z.; Xiang, Z.; Shen, X.; Li, W. Mass Transfer Model of Oriented Silicon Steel Coil during the First Soaking in Annular Furnace. *Silicon* **2023**, *15*, 269–284. [CrossRef]

10. Xia, T.; Xiang, Z.; He, Z.; Hu, S.; Luo, Z. Simulation of temperature distribution in the oriented silicon steel coil in the heating stage of annealing process. *Appl. Therm. Eng.* **2019**, *147*, 707–717. [CrossRef]
11. Fan, L.; Zhao, X.; Zhu, R.; He, J.; Zhang, Y. Effect of heating rate of final annealing stage on secondary recrystallization in grain-oriented silicon steel. *Metall. Res. Technol.* **2020**, *117*, 607. [CrossRef]
12. He, Q.; Nie, J.; Zhang, S.; Xiao, W.; Ji, S.; Chen, X. Study of Transformer Core Vibration and Noise Generation Mechanism Induced by Magnetostriction of Grain-Oriented Silicon Steel Sheet. *Shock Vib.* **2021**, *2021*, 8850780. [CrossRef]
13. Wang, C. Research and Manufacture of 110kV Power Transformer with Ultra-Lower Noise Level. *Transformer* **2021**, *58*, 7–9. [CrossRef]
14. Chen, M. Development of OSFPSZ-650000/400 Large Capacity Low-noise Transformer. *Transformer* **2022**, *59*, 1–6. [CrossRef]
15. Wu, M.; Hu, Z.; Mu, H.; Nie, J. The Development and Application of Low Magnetostriction Grain-Oriented Silicon Steel. *Transformer* **2017**, *54*, 32–35. [CrossRef]
16. Yabumoto, M.; Arai, S. Recent Development in Grain-Oriented Electrical Steel with Low Magnetostriction. *J. Mater. Eng. Perform.* **1997**, *6*, 713–721. [CrossRef]
17. Ushigami, Y. Secondary recrystallization in grain-oriented silicon steel. *Mater. Sci. Eng.* **2021**, *1121*, 012019. [CrossRef]
18. Song, H.; Wang, Y.; Esling, C.; Wang, G.; Liu, H. The role of grain colony on secondary recrystallization in grain-oriented electrical steel: New insights from an original tracking experiment. *Acta Mater.* **2021**, *206*, 116611. [CrossRef]
19. Kim, T.Y.; Kim, H.K.; Jeong, Y.K.; Ahn, Y.K.; Shim, H.S.; Kwon, D.; Hwang, N.M. Ex-Situ Time Sequential Observation on Island and Peninsular Grains in Abnormally Growing Goss Grains in Fe–3%Si Steel. *Met. Mater. Int.* **2020**, *26*, 1200–1206. [CrossRef]
20. Džubinský, M.; Kováč, F. Microstructure and texture development of Fe–3%Si GO steel during high temperature annealing. *J. Magn. Magn. Mater.* **2003**, *254–255*, 388–390. [CrossRef]
21. Harase, J.; Shimizu, R.; Kim, J.K.; SooWoo, J. The role of high energy boundaries and coincidence boundaries in the secondary recrystallization of grain-oriented silicon steel. *Met. Mater.* **1999**, *5*, 429–435. [CrossRef]
22. Kumano, T.; Haratani, T.; Ushigami, Y. The Relationship between Primary and Secondary Recrystallization Texture of Grain Oriented Silicon Steel. *ISIJ Int.* **2002**, *42*, 440–448. [CrossRef]
23. Du, P.; Zhang, N.; Hou, D.; He, Q.; Nie, J.; Meng, L. Effects of working magnetic flux density and DC bias on the iron loss of grain-oriented electrical steel sheets with different thicknesses. *Chin. J. Stereol. Image Anal.* **2020**, *25*, 339–345. [CrossRef]
24. Jahangiri, M.R.; Bayani, H.; Ardestani, M.; Mehdizadeh, M. Core loss reduction in grain oriented silicon steel sheets by two-sided laser scribing in the presence of a magnetic field. *J. Alloys Compd.* **2021**, *891*, 162080. [CrossRef]
25. Zhong, W. *Ferromagnetism*, 3rd ed.; Science Press: Beijing, China, 1998; pp. 306–308.